LA-9538-MS

2

Los Alamos National Laboratory is operated by the University of California for the United States Department of Energy under contract W-7405-ENG-36.

Designing and Testing a High-Velocity Self-Forging Fragment

Los Alamos National Laboratory
Los Alamos, New Mexico 87545

LA-9538-MS

UC-45
Issued: October 1982

Designing and Testing a High-Velocity Self-Forging Fragment

S. P. Marsh

Los Alamos National Laboratory
Los Alamos, New Mexico 87545

DESIGNING AND TESTING A HIGH-VELOCITY SELF-FORGING FRAGMENT

by

S. P. Marsh

ABSTRACT

An explosive system has been designed to propel a 215-g mild steel self-forging fragment at a velocity of 6 km/s. The design was obtained using the hydrodynamic code PETRA. Flash radiography and penetration results are reported for experiments based on this design.

INTRODUCTION

To test the vulnerability of reentry bodies to high-velocity metal fragments, we need driver systems capable of accelerating metal projectiles to velocities up to 6 km/s. Two-stage light gas guns have the velocity capability, but at present there is no such device that can be used to shoot at a large explosive charge (>2 kg). Many explosive-driven systems, such as shaped charges, also have the velocity capability, but none have been designed to produce nearly spherical metal fragments at the required high velocity. Therefore, we have undertaken the design of an explosive-driven system to produce a roughly spherical steel fragment traveling at 6 km/s.

The approach we used to produce a high-velocity fragment explosively was similar to that used in Misznay-Schardin systems. In these systems a thin, slightly cupped plate (or liner) of metal is accelerated by a high-explosive charge against its convex face. As the liner travels to a target, the velocity gradients imparted to it by the high explosive cause it to forge into a consolidated shape more appropriate for penetrating armor. These devices are sometimes called self-forging fragments (SFF). The diameter and mass of these systems are usually limited by the mode of delivery. The required fragment metal, velocity, aspect ratio, and standoff are strongly influenced by the nature of the target.

In the fragment development problem considered here, there were no limitations on the charge diameter, mass, or standoff distance, except that damage to the target should not be caused by explosive system elements other than the fragment. The self-forging of the liner into a fragment is usually accomplished by having the periphery fold forward or backward with respect to the liner center, arriving at an aerodynamically stable shape needed to travel long distances to a target without tumbling. In the design reported below, folding has not been an important element of the fragment consolidation. Instead, the entire area of the plate is accelerated to a uniform velocity and directed initially to a common point in front of the charge. This results in a mass-focused forging in which ideally no folding occurs, but only a thickening of the plate as the mass elements approach the

cylindrical axis of symmetry.* An axial velocity gradient results from this method of consolidation so that the common focal point of the velocity vectors of the liner needs to be far enough out from the charge that over-elongation of the fragment does not occur before the target is reached.

CALCULATIONS

The dimensional parameters of the design were determined by means of hydrodynamic calculations. The two-dimensional Eulerian code we used was PETRA, developed in the United Kingdom by members of the Atomic Weapons Research Establishment. This code is multimaterial with strength included, and it has a programmed burn for the high-explosive components.

The basic system we chose to study is shown in Fig. 1. The liner was mild steel, the metal for the desired fragment, with a nominal thickness of 0.16 cm. This liner was thin enough that it could be accelerated to a high velocity but thick enough that it would not be broken up by the detonating explosive. The liner faces were parallel spherical surfaces with radius of curvature R and an outer diameter d. The liner was mounted in a steel ring that assisted in supporting the liner, as well as confining the explosive products behind the liner during initial liner acceleration. The high explosive (HE) was PBX 9501, of diameter d_{HE} and thickness t_{HE}, selected because of its high Chapman-Jouget (C-J) pressure and fine grain texture that would minimize breakup of the liner. No confinement was required on the periphery of the explosive. The explosive charge was detonated simultaneously on its face opposite from the liner (over the diameter d_I indicated with a dashed line).

---

*This information was supplied by John Richter, Los Alamos National Laboratory.

The parameters for the calculations that were performed are shown in Table I. The yield strength of the liner was given a high value of 1.2 GPa in three of the problems because of the high strain rate during fragment formation.

RESULTS OF CALCULATIONS

The calculated fragment velocity was 5.7 km/s for the three problems having an explosive thickness of 10 cm, whereas in D0304 a mean velocity of 4.9 km/s was obtained with an explosive thickness of 4 cm. In the latter problem the fragment velocity ranged from 6 to 4.2 km/s from tip to tail. Placing yield strength in the liner and increasing its radius of curvature reduced this velocity gradient to nearly zero in the other calculations.

There were fragment formation effects caused both by the HE lens and HE charge diameters. Because of the relatively thin charge used in D0304, very little peripheral liner mass was reduced in velocity by the edge rarefaction in the detonated explosive. But in the systems having thicker charges, reduced peripheral liner velocities (and less convergent velocity vectors) did result to varying degrees. In Fig. 2 the slug contours are compared at 40 μs after charge initiation. Whereas the slug in D0304 contains almost all of the liner mass, the others have massive peripheral regions beginning to lag slightly. This continues to be seen at 70 μs in Fig. 3, at which time a lesser consolidation (as reflected by the polar thickness) is observed for those with the greatest peripheral lag. The most lag appears in D0305, and it is associated with the small charge and initiation surface diameters of 20.3 cm (8 in.). An improvement can be seen in D0309 where the charge diameter is 25.4 cm (10 in.), and further improvement yet is seen in D0309A where both the initiation and charge diameters are increased to 30.5 cm (12 in.).

Problem D0309A was calculated far enough in time (120 μs) that a stable fragment was obtained after 100 μs for the yield strength used. (See Fig. 4.)

EXPERIMENTS

Because of the uncertainty of the yield strength used in the calculations, we chose three systems for experiments. Not only were the parameters for problem D0309A chosen for fabrication, but two other systems were also fabricated having larger radii of curvature for the liner (40.6 and 64.0 cm). The reason for this choice was the belief that the yield strength was more likely to be too high than too low and that "overforging" of the fragment might occur. The larger radii of curvature would compensate for this overforging and result in more properly shaped fragments (near an aspect ratio of unity) at the standoff distances where radiographs were to be taken.

The liners had diameters of 15.2 cm (6 in.) and were fabricated from 1020 steel in the dead soft condition. The thicknesses of all three liners varied from approximately 0.147 cm at the periphery to 0.152 cm at the center with about 0.001 cm variation in thickness around circles equidistant from the center. No tolerances were obtained for the radii of curvature.

The method for assembling the charges is shown in Fig. 5. The liner was cemented into the mounting ring, and Composition C* explosive was then carefully hand pressed against the back of the liner to remove as much porosity as possible. The thickness of the mounting ring was chosen to be that required to make the thickness of the Composition C vanish over the liner pole when a straight edge was drawn across the mounting ring surface to smooth the Composition C. The PBX 9501** charge was then placed in contact with this surface and a P-120 plane-wave explosive lens, 30.5 cm (12

---

* Composition in wt% - 60 RDX/40 TNT, ρ_0 = 1.72 g/cm^3.

** Composition in wt% - 91 RDX/5.3 di(2-ethylhexyl) sebacate/2.1 polyisobutylene/1.6 motor oil, ρ_0 = 1.60 g/cm^3.

in.) in diameter, was placed on the back of the PBX charge. The assembly was placed on Styrofoam spacers to isolate the charges from reflected ground shocks, and the assembly elements were held compressed in a wooden stand.

This assembly is shown in Fig. 6, along with other elements of the experiment used for diagnostics. An armored container for the x-ray film cassette is seen above the explosive assembly. An aluminum plate 1.27-cm (0.5 in.) thick allows penetration of the x rays but protects the cassette from explosive shock damage. The two flash x-ray sources were 300 keV with 20-ns pulse lengths. Different mild steel targets were used in the three experiments, one of which was a cylinder 30.5 cm (12 in.) in diameter and 30.5 cm (12 in.) long, shown in Fig. 6. The target and x-ray cassette were placed at a greater standoff for Exp. 1628 because of the greater distance expected to be necessary for consolidation of the liner.

A summary of the parameters used in these experiments is given in Table II, including distances from the charge face to the center fiducial (d_{fid}) on the radiographs, the times of the two x-ray exposures after detonation time (T_1 and T_2), and a description of the numbers and thicknesses of the targets in each experiment and the standoff of the target face from the charge face (SO).

EXPERIMENTAL RESULTS

The x-radiographs of the fragments are shown in Figs. 7-9. In all three radiographs, ductile deformation appears to be occurring at radiographic times. No evidence of brittle fracture exists at these times. However, all of the fragments were continuing to deform at the times of the radiographs.

Because no other major fragment pieces were observed in the entire area in the original radiographs (14 in. × 17 in.), we assumed that essentially all of the liner mass was in these fragments. The degree of consolidation is highest for the liner of shortest radius of curvature (Exp. 1626) and is

least for the liner of greatest radius of curvature (Exp. 1628). The aspect ratio of length to diameter (AR) of the fragments and the distance traveled at that time (d_{AR}) are given in Table III. The velocity (V) of the center of each of the fragments was nominally 6.0 km/s at radiographic times, although consolidation is still occurring and increasing velocity gradients will occur. The radiographs of Exps. 1626 and 1627 show no evidence of significant deviation from axial symmetry of the fragment. However, the liner having the largest radius of curvature gave a fragment in Exp. 1628 that did have a nonsymmetric hole visible near the leading edge. This asymmetry may arise from the fragment having traveled twice as far as those of the other two experiments when the radiograph was taken, or, perhaps from the lack of uniformity of density of the hand-packed Composition C explosive.

A photograph of the recovered mild steel targets is shown in Fig. 10, and a summary of the target penetrations is given in Table III. Only fragments were recovered from the front 2-in steel target plate of Exps. 1626 and 1627. The second 2-in steel plate of Exp. 1626 had a 14-cm-diameter hole in it, and the third plate had a 12-cm-diameter hole and was badly spalled. The reason for the large diameter of this penetration is not understood in view of the fact that the fragment was only 3 cm in diameter and still elongating when only 25 cm from the target. The length of the fragment must have contributed in some way to this penetration diameter.

The second target element of Exp. 1627 was 10 cm thick and had a 5-cm-diameter penetration. The back spalled layer had not been penetrated.

The target of Exp. 1628 was not penetrated. It had an impact crater that was approximately 15 cm in diameter and 6 cm deep. The fragment was approximately 7 cm in diameter just prior to impact so a large diameter crater was to be expected.

CONCLUSIONS

We have successfully designed, by use of the hydrocode PETRA, a mass-focused self-forging-fragment explosive system. In designing experiments to test the calculations, we made allowance for the uncertainty of the yield strength of mild steel at high strain rates. From the results of the experiments, we determined that the yield strength used in the calculations was too high and did not allow enough forging to occur. The fragment continued to deform during the time of observation for all of the experiments.

The parameters of Exp. 1627 were successful in producing a steel fragment having an aspect ratio of unity for a target at a standoff of 90 cm. This fragment had a mass of 217 g and a velocity over 6 km/s. The fragment velocity was higher than the calculated value (5.7 km/s) because the explosive lens added confinement to the explosive system.

To achieve massive steel slugs having a velocity of 6 km/s using the design presented here, we found it most desirable to use a large diameter (30.5-cm) system with a relatively large radius of curvature of the liner (40.6 cm). Either reducing the HE diameter or reducing the radius of curvature of the liner increases the likelihood of slug instability caused by peripheral lag and axial velocity gradients, respectively. The following additional inferences are drawn from this and other work: lower velocity slugs can be produced by substituting HE having a lower C-J pressure than the PBX 9501 used in these calculations. Thickening the liner will also result in lower velocities and increased slug masses. Slug masses can be decreased by just reducing the diameter of the liner without changing the explosive system.

TABLE I

Parameters and Results for Self-Forging Fragment Calculations

	High Explosive			Liner				Fragment
Problem	d_{HE} (cm)	t_{HE} (cm)	d_I (cm)	d (cm)	R (cm)	Mass (g)	Yield Str. (GPa)	Velocity (km/s)
D0304	20.3	4	20.3	12.70	16.1	160	0	4.9
D0305	20.3	10	20.3	15.24	25.4	228	1.2	5.7
D0309	25.4	10	20.3	15.24	25.4	228	1.2	5.7
D0309A	30.5	10	30.5	15.24	25.4	228	1.2	5.7

TABLE II

Experimental Parameters for Three Self-Forging Fragment Experiments

	Liner		X-radiographs			Targets		
Experiment	Mass (g)	R (cm)	d_{fid} (cm)	T_1 (μs)	T_2 (μs)	Number	Thick. (cm)	SO (cm)
1626	223.2	25.4	60.3	156.2	183.1	3	5.1 ea	89.1
1627	217.6	40.6	61.0	136.5	161.5	1 1	5.1 ea 10.2 ea	91.4
1628	217.8	61.0	121.9	236.5	261.5	1	30.5 ea	152.4

TABLE III

Experimental Results

	Fragment				Target
Experiment	Mass (g)	V (km/s)	AR	d_{AR} (cm)	Hole Diam. (cm)
1626	223	6.0 [a]	3.2	/ 66	14/12
1627	217	6.0	0.6	/ 71	5
1628	217	6.1	0.6	/ 127	15 [b]

[a] Inferred from the gradient determined from that part of the fragment visible in the second exposure.

[b] Impact crater diameter.

Figure 1. Self-forging fragment system on which hydrodynamic calculations were performed.

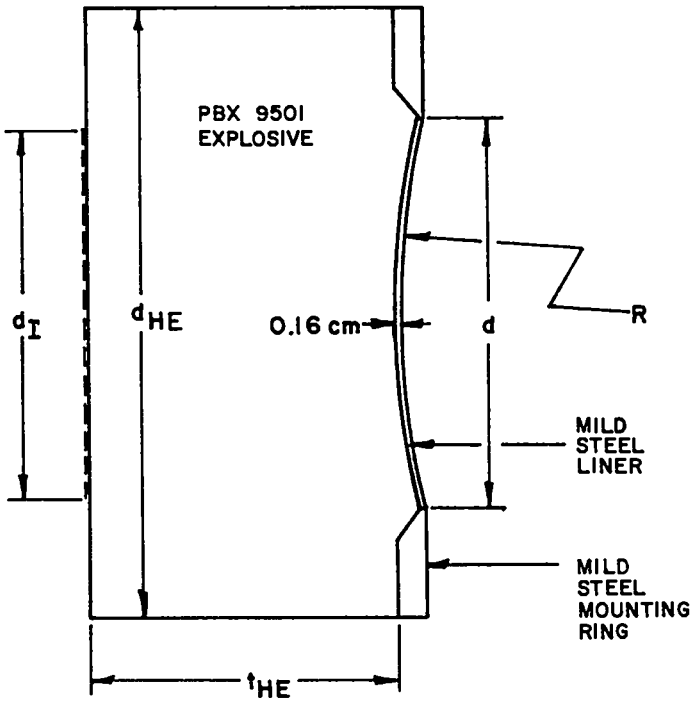

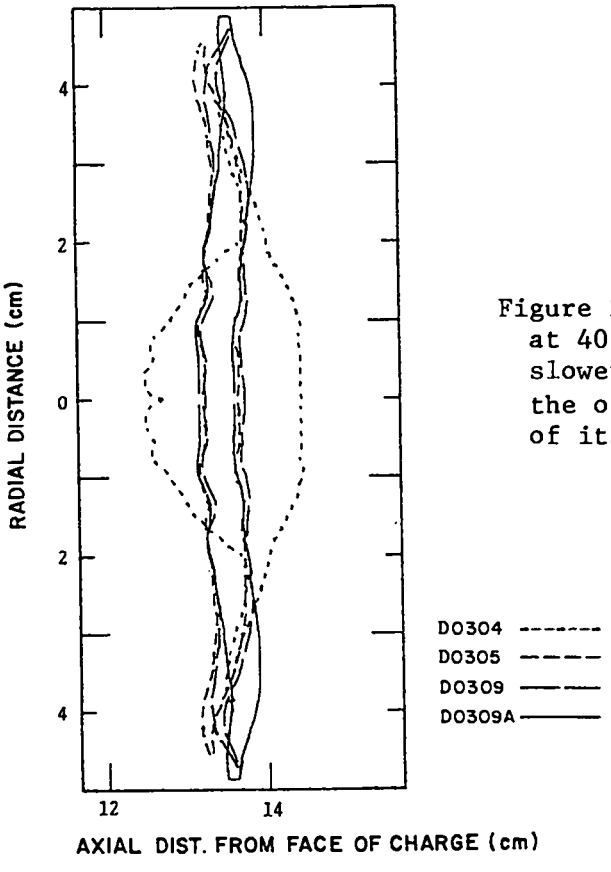

Figure 2. Comparison of fragment contours at 40 μs after HE initiation. The slower-moving fragment of D0304 overlays the other contours at this time because of its shorter HE burn time.

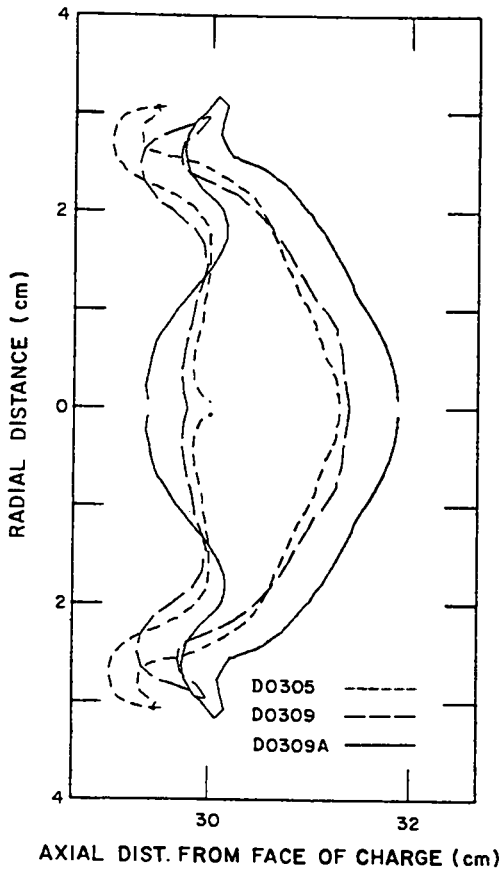

Figure 3. Comparison of fragment contours at 70 μs after HE initiation.

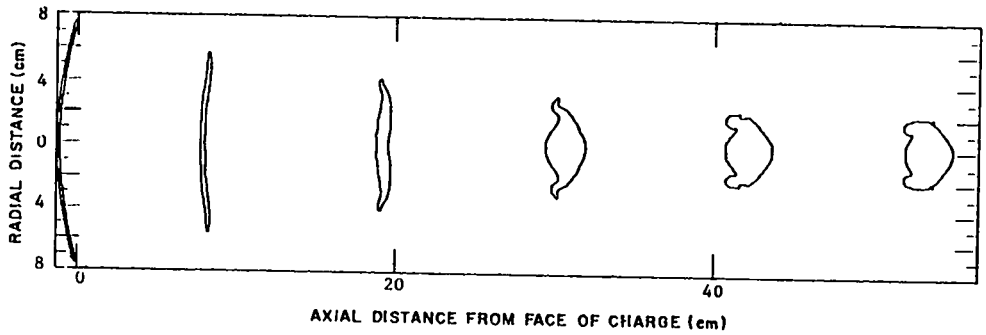

Figure 4. Fragment formation for problem D0309A. Liner/fragment contours are shown at times after HE initiation of 0, 30, 50, 70, 90, and 110 μs.

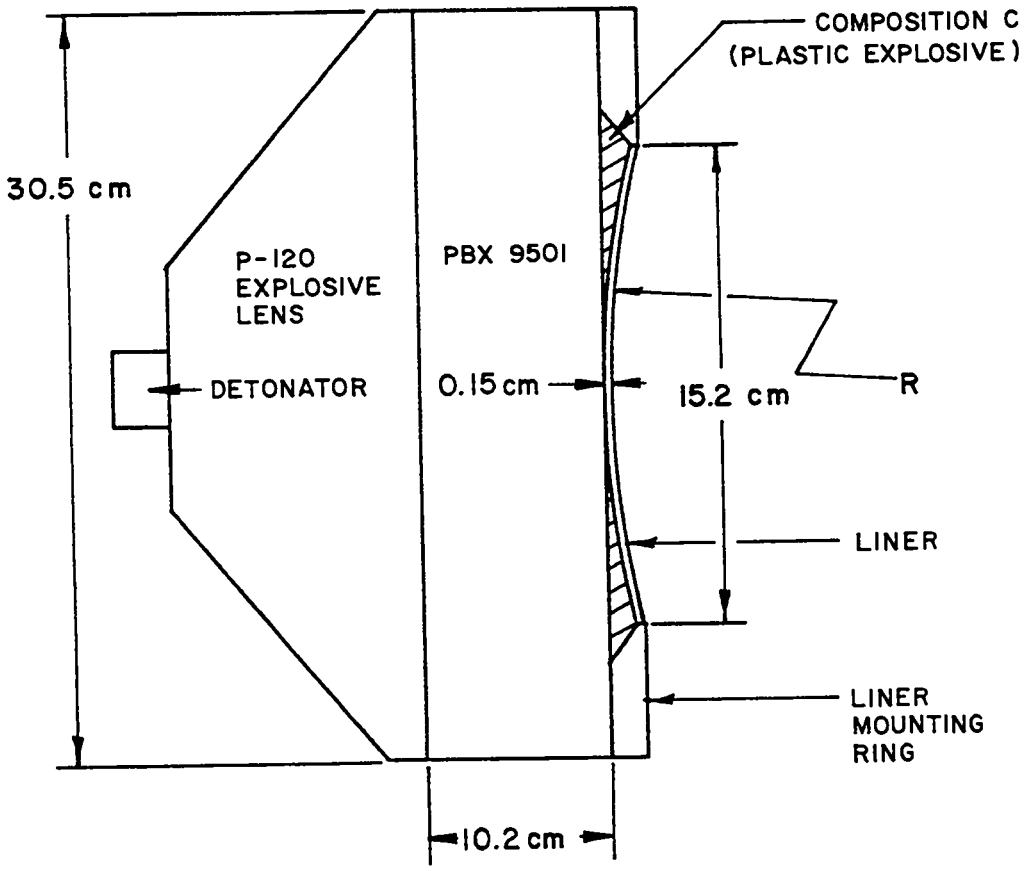

Figure 5. Self-forging fragment system as fabricated.

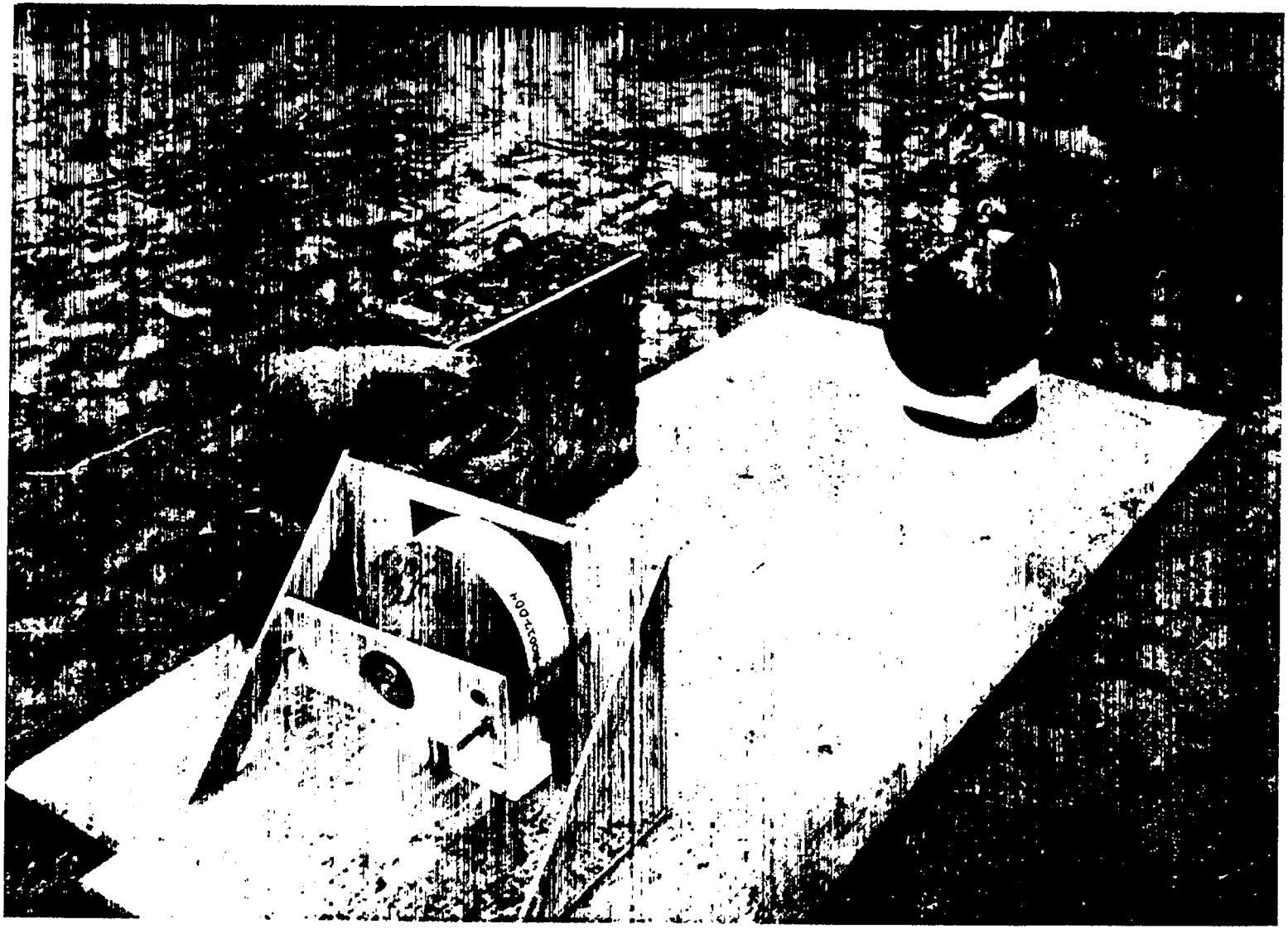

Figure 6. Experimental set-up for testing self-forging fragment charges.

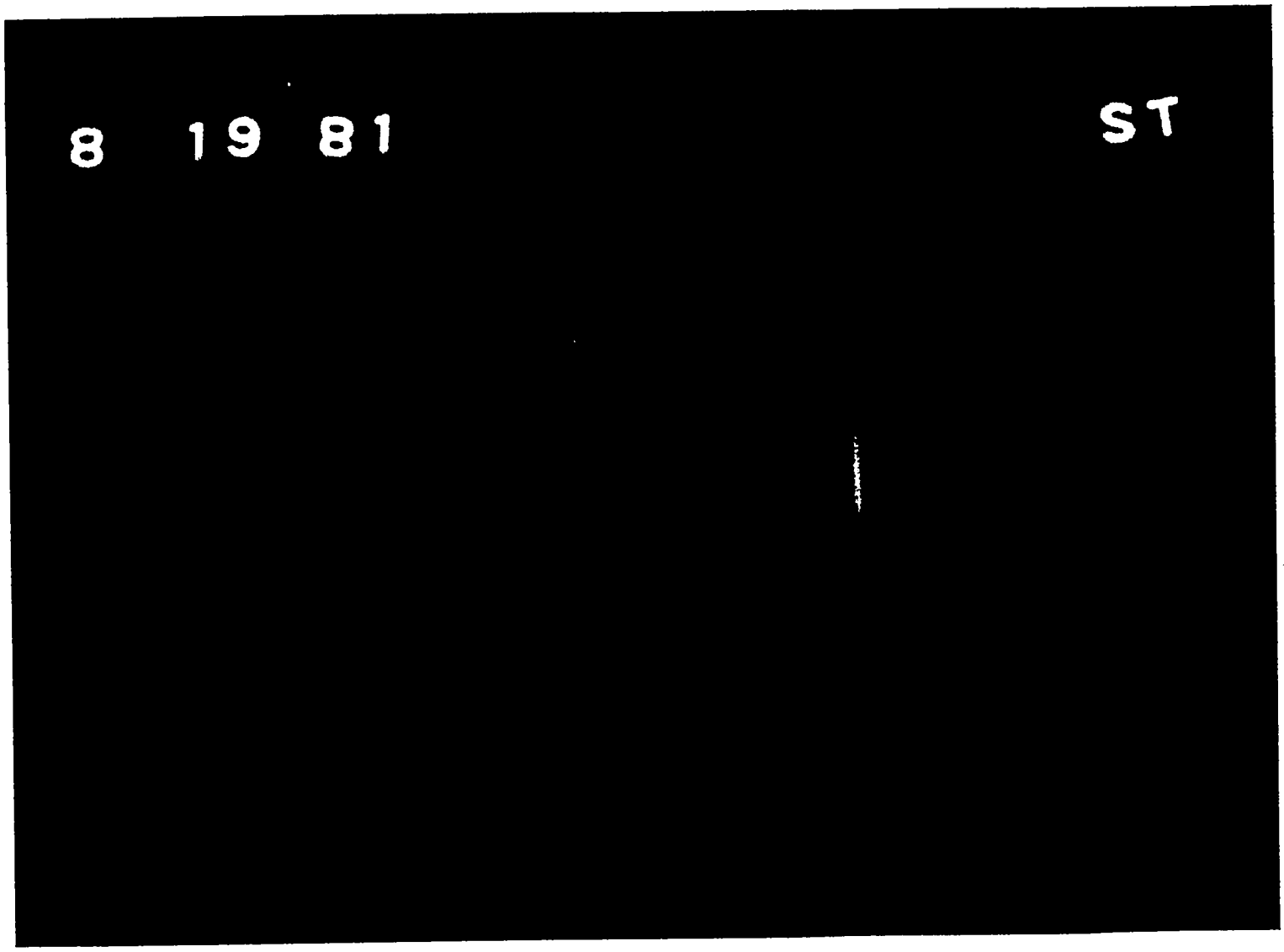

Figure 7. X radiograph of the fragment in Exp. 1626. The spacing of the space fiducials is 7.5 cm.

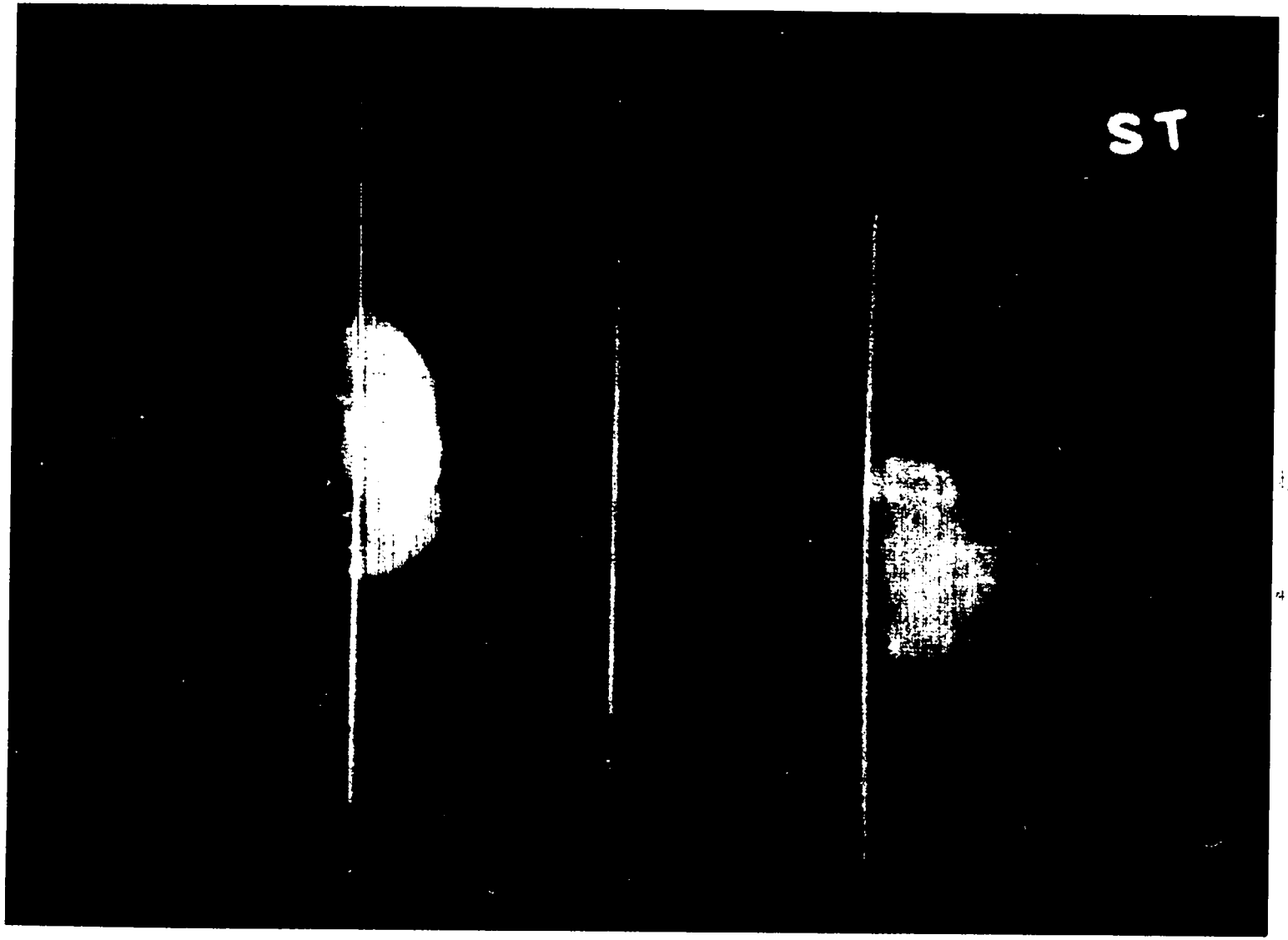

Figure 8. X radiograph of the fragment in Exp. 1627. The spacing of the space fiducials is 7.5 cm.

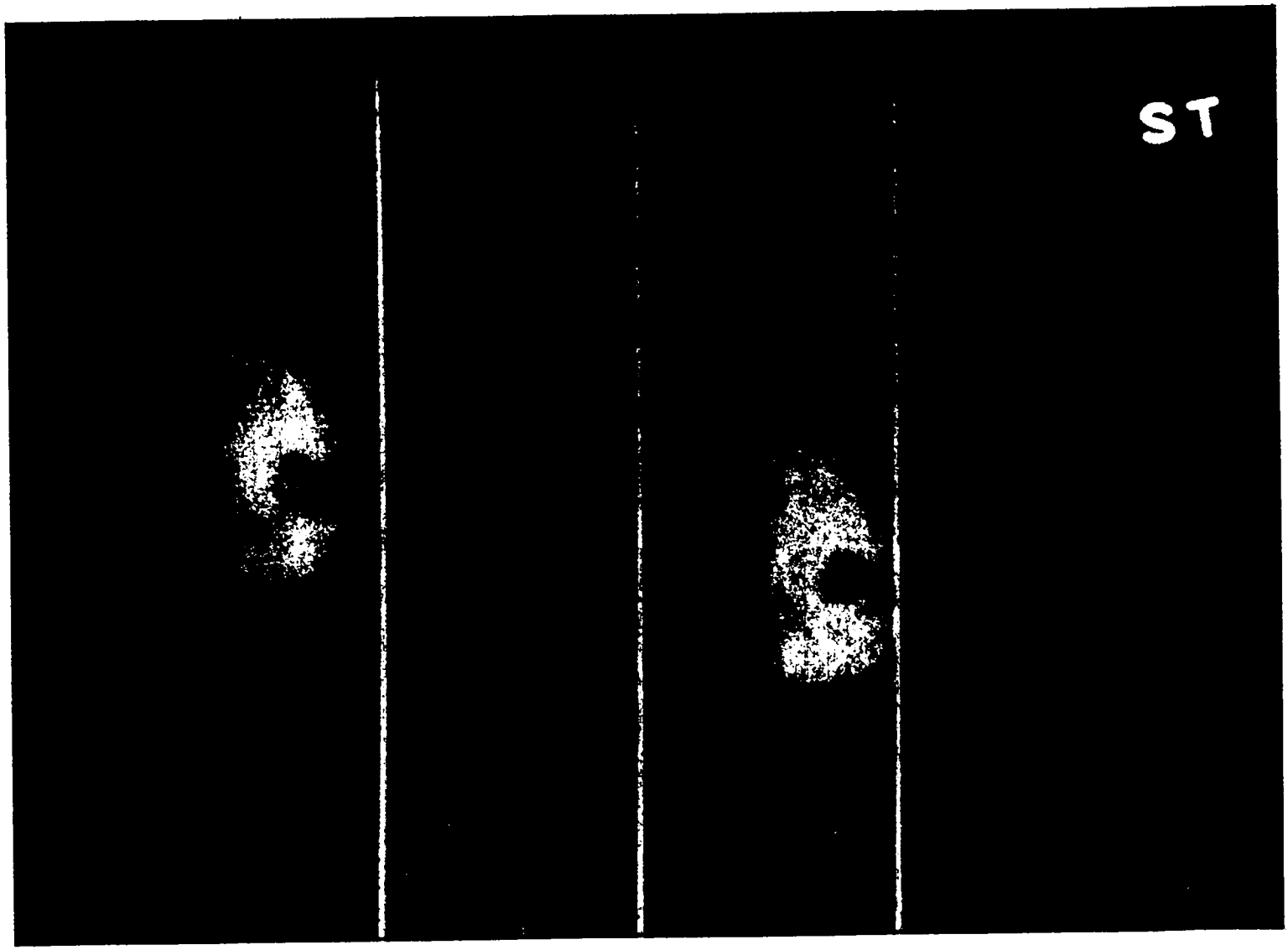

Figure 9. X-radiograph of the fragment in Exp. 1628. The spacing of the space fiducials is 7.5 cm.

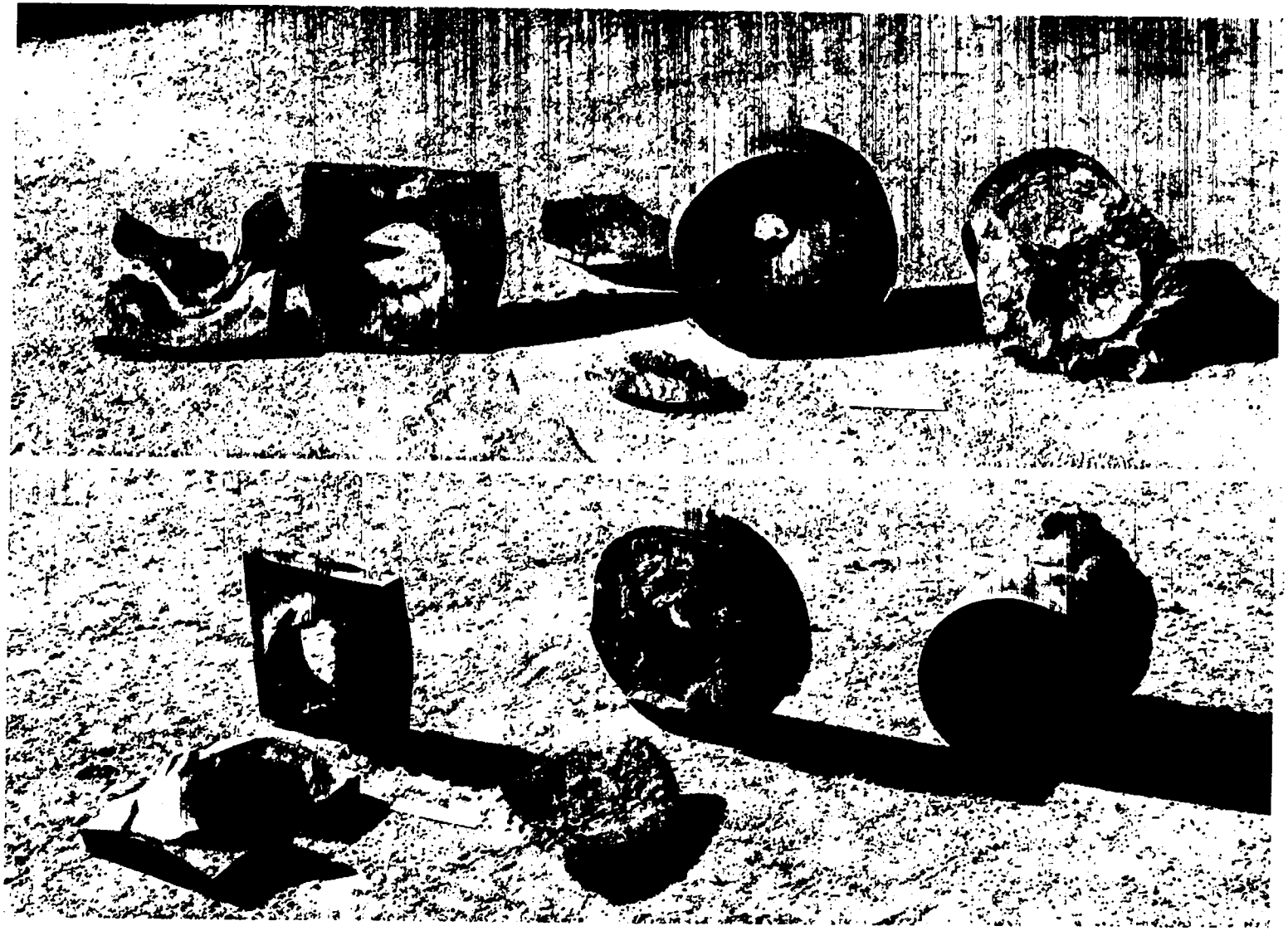

Figure 10. Recovered steel targets from Exp. 1626 (left), Exp. 1627 (center), and Exp. 1628 (right). The fragment entry side of the targets is shown above and the back of the targets below.

Printed in the United States of America
Available from
National Technical Information Service
US Department of Commerce
5285 Port Royal Road
Springfield, VA 22161

Microfiche (A01)

Page Range	NTIS Price Code	Page Range	NTIS Price Code	Page Range	NTIS Price Code	Page Range	NTIS Price Code
001-025	A02	151-175	A08	301-325	A14	451-475	A20
026-050	A03	176-200	A09	326-350	A15	476-500	A21
051-075	A04	201-225	A10	351-375	A16	501-525	A22
076-100	A05	226-250	A11	376-400	A17	526-550	A23
101-125	A06	251-275	A12	401-425	A18	551-575	A24
126-150	A07	276-300	A13	426-450	A19	576-600	A25
						601-up*	A99

*Contact NTIS for a price quote.

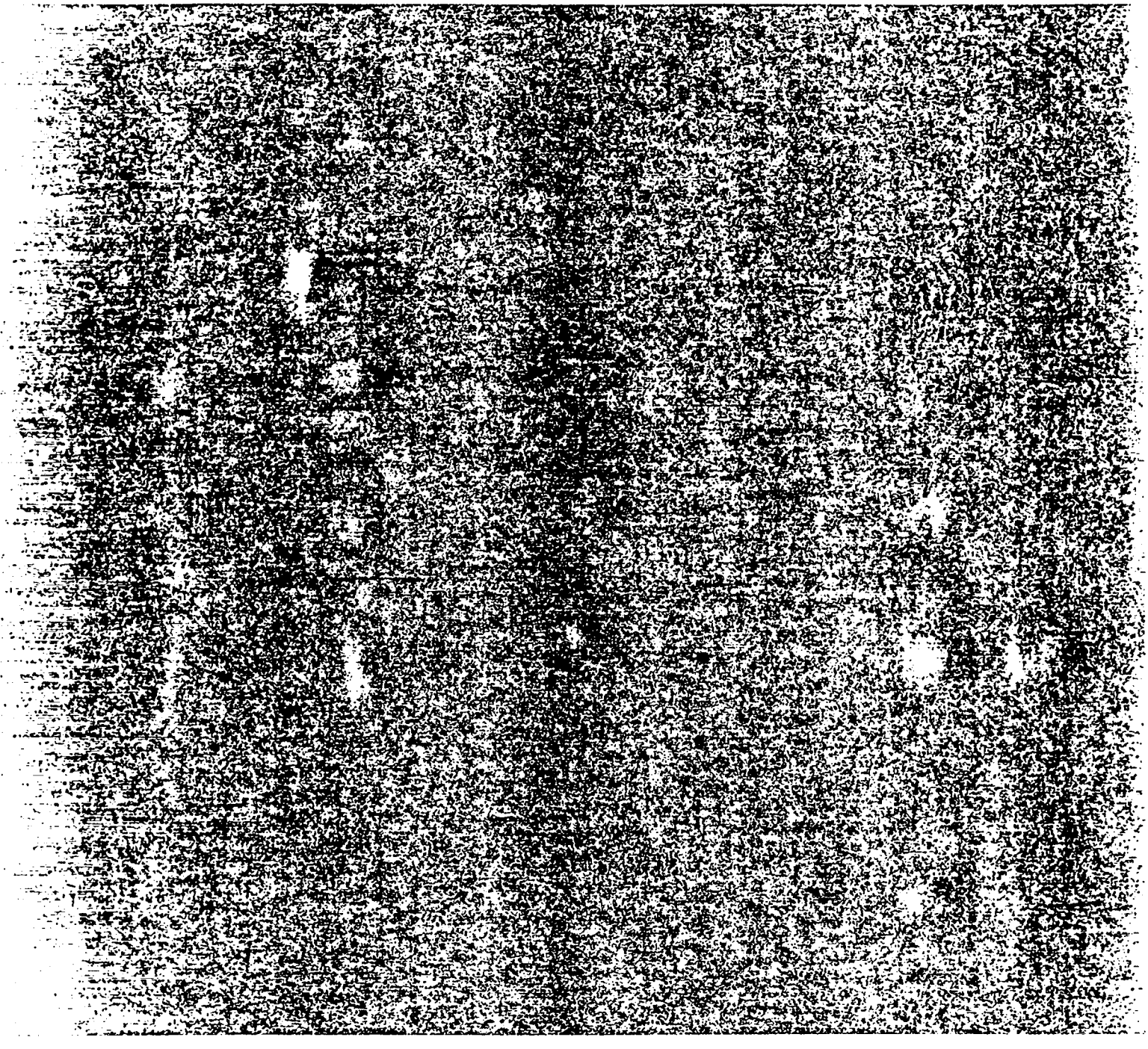

Los Alamos